Journal of Solid State Chemistry 181 (2008) 2918–2923

Contents lists available at ScienceDirect

Journal of Solid State Chemistry

journal homepage: www.elsevier.com/locate/jssc

Uncontrollable expansion of $PbZn_{1/3}Nb_{2/3}O_3$–$PbTiO_3$ perovskite ⇒ pyrochlore transition during spark plasma sintering: Mechanism proposal using infinite periodic minimal surfaces

T. Hungria [a,b], A. Castro [b], M. Alguero [b], J. Galy [a,*]

[a] Centre d'Elaboration de Matériaux et d'Etudes Structurales (CEMES-CNRS), 29, rue Jeanne Marvig, BP 94347, 31055 Toulouse, France
[b] Instituto de Ciencia de Materiales de Madrid (ICMM, CSIC), Cantoblanco, 28049 Madrid, Spain

ARTICLE INFO

Article history:
Received 14 April 2008
Received in revised form
8 July 2008
Accepted 10 July 2008
Available online 22 July 2008

Keywords:
Spark plasma sintering
Perovskite–pyrochlore transition
Lone pair
Structural mechanism
Infinite periodic minimal surfaces

ABSTRACT

The $PbZn_{1/3}Nb_{2/3}O_3$–$PbTiO_3$ phase (PZN–PT) prepared by mechanosynthesis exhibits interesting relaxor properties when transformed into nanostructured ceramic by spark plasma sintering. When trying to obtain denser ceramic to enhance physical properties, the PZN–PT phase transformation from perovskite to pyrochlore structure induces the graphite die explosion. An explanation of this phenomenon is based on the reorganization of the lone pairs corresponding to Pb^{2+} cations into the large cavities of pyrochlore network, inducing an important cell volume increase, together with the speed of transformation depicted in the light of infinite periodic minimal surfaces describing the perovskite (P-surface) and the pyrochlore (F-surface) networks, respectively.

1. Introduction

In recent years much attention has been paid to lead-based relaxor ferroelectric $Pb(B,B')O_3$ with $B,B' = Ti$, Nb, W, Mg, Zn, compounds with the perovskite structure. Indeed, these materials present interesting dielectric, ferroelectric and piezoelectric properties that could, potentially, be extremely useful in many electromechanical devices, such as sensors and actuators [1,2]. Lead zinc niobate, $Pb(Zn_{1/3}Nb_{2/3})O_3$ (abbreviated as PZN) is one of these compounds that exhibits a partially disordered arrangement of the Zn^{2+} and Nb^{5+} cations in the *B*-site of the ABO_3 perovskite structure, Pb being in the oxygenated cuboctahedron centred in the middle of the cubic cell. PZN undergoes a rhombohedral (ferroelectric) to cubic (relaxor) phase transition at temperatures around 140 °C [3], although a more recent study has reported a significantly lower transition temperature [4].

Recently, the solid solutions with a morphotrophic phase boundary (MPB) have attracted a lot of attention owing to their unusual high dielectric and piezoelectric properties associated with a monoclinic phase at the MPB [5] and a polarization rotation among the phases [6,7]. In the case of the solid solution between the PZN rhombohedral phase and the $PbTiO_3$ (PT) tetragonal phase, represented by PZN–PT, there is an MPB close to 0.1 PT. It was found that the ⟨001⟩ poled rhombohedral crystals close to the MPB exhibit piezoelectric and electromechanical properties significantly higher than those of the best lead zirconate titanate (PZT)-based piezoelectric ceramics. Unfortunately, pure perovskite PZN-based ceramics are very difficult to prepare by conventional routes because of the high polarizability of Pb^{2+} cation and its interaction with Zn^{2+}, resulting in the destabilization of the perovskite phase, which rapidly turns into a pyrochlore-type phase [8]. The powder perovskite close to the MPB composition could only be obtained by high-pressure methods [9] and, in our group, as a nanocrystalline powder by mechanosynthesis [10]. However, even if the perovskite is obtained by alternative synthesis methods, the phase is not stable under heating, decomposing into pyrochlore, PbO and ZnO during the sintering process in air, PbO-rich atmosphere and even under hot pressing [7]. Due to the good results obtained while sintering other electroceramics from mechanosynthesized powders [11,12] the spark plasma sintering (SPS) technique was used as an alternative. By combining these unconventional methods, applied for the first time to the PZN–PT solid solution, nanostructured materials with a grain size of 15–20 nm have been successfully processed and the results on electrical properties indicate that the relaxor state does exist in these nanostructured materials [13]. However, contrary to what has been observed in other perovskite-based systems, when the temperature exceeds 700 °C to get a higher densification, the explosion of the graphite die is observed.

* Corresponding author.
E-mail address: galy@cemes.fr (J. Galy).

0022-4596/$ - see front matter © 2008 Elsevier Inc. All rights reserved.
doi:10.1016/j.jssc.2008.07.014

The aim of this work is to provide an explanation about the structural processes taking place inside the PZN–PT nanometric crystals during the SPS step and to see how they fit in with this uncontrollable and sudden expansion of the pellet causing graphite die explosion. As a result, particular attention will be paid to the role of Pb^{2+} lone pairs [14,15]. Furthermore, the description based on the infinite periodic minimal surfaces (IPMS) of perovskite and pyrochlore-related networks presented by Andersson et al. [16] using the differential geometry, will be used and a mechanism accounting for the violence of the phase transition will be proposed. A minimal surface is most simply defined in the context of differential geometry as a surface of zero mean curvature. A great number of structures can be described by a very limited number of minimal surfaces. The IPMSs corresponding to both primitive P and face-centred F surfaces moulded in plastic are depicted in Fig. 1 and it is also shown how they accommodate on one side the ReO_3 network of ABO_3 perovskite and the A atoms inserted into the labyrinths (Fig. 1a). Similar description is used for $[(Al, Si)O_2]_n$ network of the mineral faujasite (Fig. 1b). The structure of the faujasite $(Al, Si)_2O_7$ is closely related to that of the pyrochlore (Na, Ca)Nb_2O_6F, in the second one the six-fold rings of the faujasite are replaced by the BO_6 octahedra of the $[B_2O_6]_n$ network of the pyrochlore. The final pyrochlore structure consist of the interpenetration of the $[B_2O_6]_n$ and A_2F networks, resulting in the same space group as in the case of faujasite.

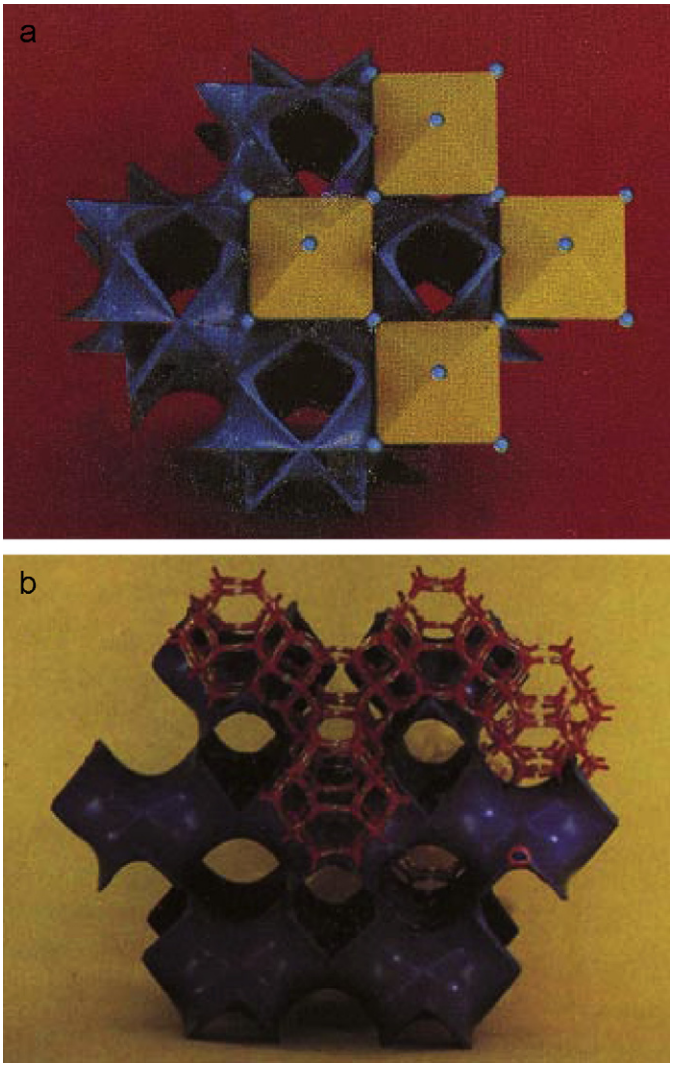

Fig. 1. Infinite periodic minimal surface (blue plastic form): (a) primitive, with the BO_6 octahedra (yellow) of the ReO_3 network of ABO_3 perovskite, the empty labyrinths accommodating the A atoms and (b) face-centred, with the rings of $[(Al, Si)O_2]_n$ built up by $(Al, Si)O_4$ tetrahedra (red); in the case of pyrochlore the $[B_2O_6]_n$ network substitutes for the $[(Al, Si)O_2]_n$ one and is interpenetrated by the A_2O antifluorite network inserted into the labyrinths. Courtesy of Andersson et al. [16].

2. Experimental

Mechanosynthesis of 0.92PZN–0.08PT has already been reported [10]. Ceramic pellets were obtained using the SPS technique on a Syntex 2080 machine set up by CEMES for "Plate-forme Nationale de Frittage Flash/CNRS" in Toulouse[1]. For each pellet, a weighed amount of powder was inserted into an 8 mm inner diameter carbon die to achieve a 3 mm thick high ceramic. The pellet, under increasing uniaxial pressure up to 100 MPa was heated to the final temperature (T_f) via 3.3 ms DC electric pulses according to the following protocol: 20–(T_f−100) °C with a heating rate of 100 °C min^{-1}, and the last 100 °C in 2 min followed by 3 min isothermal holding time at T_f and 100 MPa before rapid quenching. Compaction of the pellets was followed with a dilatometer to record the linear shrinkage (ΔL) of the sample as a function of temperature and/or time.

X-ray diffraction patterns of powder and pellets were recorded at room temperature in the 2θ range 10–60° (2θ) in steps of 0.04° and counting rates of 10 s, with a SEIFERT XRD 3000T/T diffractometer using a graphite monochromatized Cu$K\alpha$ radiation. Unit cell parameters were derived from these data after hkl indexing of all diffraction peaks and least-square refinement using the CELREF program.

Volumic mass measurements were carried out using Micromeritics Accupyc 1330 helium pycnometer.

3. Results

It was possible to compact the perovskite by SPS with, however, an upper limit of 650 °C and under 100 MPa. XRD patterns of the materials prepared by SPS under different conditions are shown in Fig. 2 and densities and compositions are listed in Table 1.

Thermal decomposition of the perovskite was observed after processing by SPS at temperatures higher than 500 °C with an increasing quantity of the pyrochlore phase at increasing temperature. Attempts to increase temperature and pressure above 700 °C and 100 MPa to stabilize the perovskite phase led, systematically, to a sudden violent explosion of the carbon die. Fig. 3 depicts the shrinkage curves recorded in situ. They correspond to different sintering conditions, leading to explosive experiments when the pressure and/or temperature of the sintering step is increased. A thorough investigation has been carried out to understand this limitation not observed in other systems.

XRD patterns of the perovskite phase prepared by mechanosynthesis and the product with a pyrochlore structure which is obtained from the mechanosynthesized powder after thermal treatment of 700 °C, are shown in Fig. 4. A small quantity of ZnO and perovskite phase can be identified as secondary phases of the thermal decomposition of the 0.92PZN–0.08PT perovskite. Refinements of XRD powder patterns of both perovskite and pyrochlore phases are carried out according to the $Pm3m$ and $Fd3m$ space groups, respectively. With respect to perovskite, no

[1] PNF2/CNRS ? MHT, Université Paul Sabatier, Toulouse, France. Established by P. Millet, P. Rozier, J. Galy, 2003–2004.

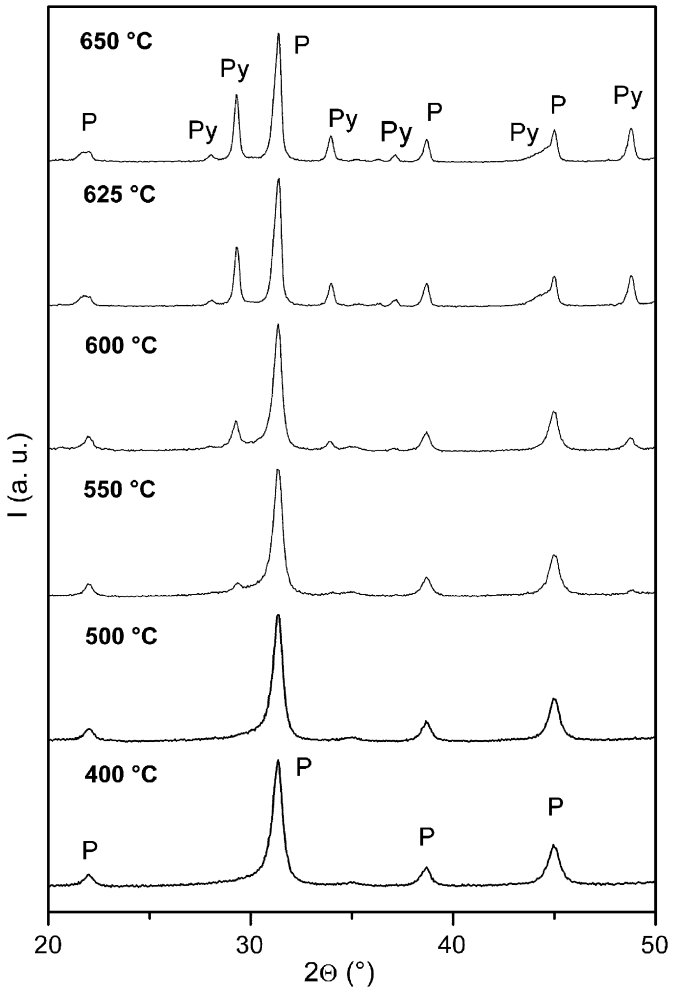

Fig. 2. XRD patterns of materials processed by SPS at different temperatures from the mechanosynthesized 0.92PZN–0.08PT perovskite.

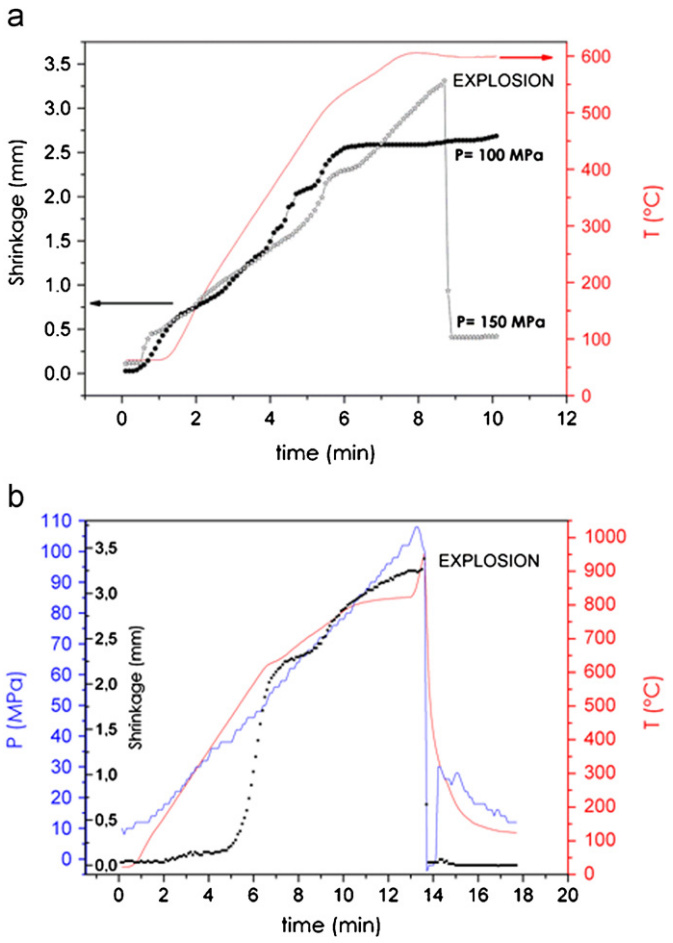

Fig. 3. Shrinkage curves recorded during SPS processing of the 0.92PZN–0.08PT materials from mechanosynthesized precursors using different final sintering conditions: (a) 600 °C under different pressures and (b) 1000 °C under 125 MPa.

Table 1
Densities and percentage of pyrochlore phase for materials processed by SPS at different temperatures from the mechanosynthesized 0.92PZN–0.08PT perovskite

Temperature (°C)	ρ (g cm^{-3})	ρ relative (%)	Pyrochlore percentage (%)
400	5.26	62.5	–
500	5.58	66.3	–
550	5.91	70.2	5
600	6.77	80.4	11
625	7.62	90.5	24
650	7.61	90.5	30

differences can be found between the XRD pattern derived from the rhombohedral ($R3m$) and the cubic ($Pm3m$) structural model. As a result, the simplest structure is used. Comparison of structural data in both phases (Table 2) shows that the pyrochlore cell volume is bigger than the perovskite variety, this volume increase being around 13%.

4. Discussion

It is worth pointing out first that to try and promote a mechanism regarding this violent explosion of the carbon die vessel under uniaxial pressure, is tantamount to emphasizing the role of the lone pair belonging to Pb^{2+}. It was demonstrated in a number of structures involving the so-called "lone pair elements" M^* ($M^* = As^{3+}$, Se^{4+}, Sn^{2+}, Sb^{3+}, Te^{4+}, I^{5+}, Xe^{6+}, Tl^{+}, Pb^{2+}, Bi^{3+}), that the room occupied by the lone pair, represented by E, is roughly the same as an oxygen, or K^+ or Ba^{2+} [14,15]. The stereochemistry of these M^* (CN = 3, 4, 5) is decomposed into atom positions and the sphere of influence of its lone pair E whose centre is located opposite coordination bonds, varies with the M^* nature. For Pb^{2+} this distance is estimated to be approx. 0.7–0.8 Å. So the formula of the general lead perovskite ($PbMO_3$) is better expressed in structural terms as $(PbE)MO_3$; (PbE) shows a similar volume occupancy as K^+ or Ba^{2+} for example in the networks of $KNbO_3$ and $BaTiO_3$ perovskites. The lone pair of the Pb^{2+} atoms fills the same space as an oxygen atom, something which is quite difficult in the case of the position A of the perovskite (a fairly dense structure). For this reason in the $(PbE)MO_3$ perovskite the interactions between the A (Pb^{2+}–E) and B cations are too strong producing the instability of the perovskite. As a result the Pb^{2+} cation is displaced from position A of the ideal perovskite, resulting a Pb^{2+} coordination which is similar to the one in the red PbO structure [17]. It seems reasonable that the interaction between A and B increase with the temperature decreasing the stability of the perovskite. After transformation into pyrochlore, the structural formula becomes $(PbE)_2M_2O_6$ and must be compared to the one of mineral pyrochlore $(NaCa)Nb_2O_6F$, described previously.

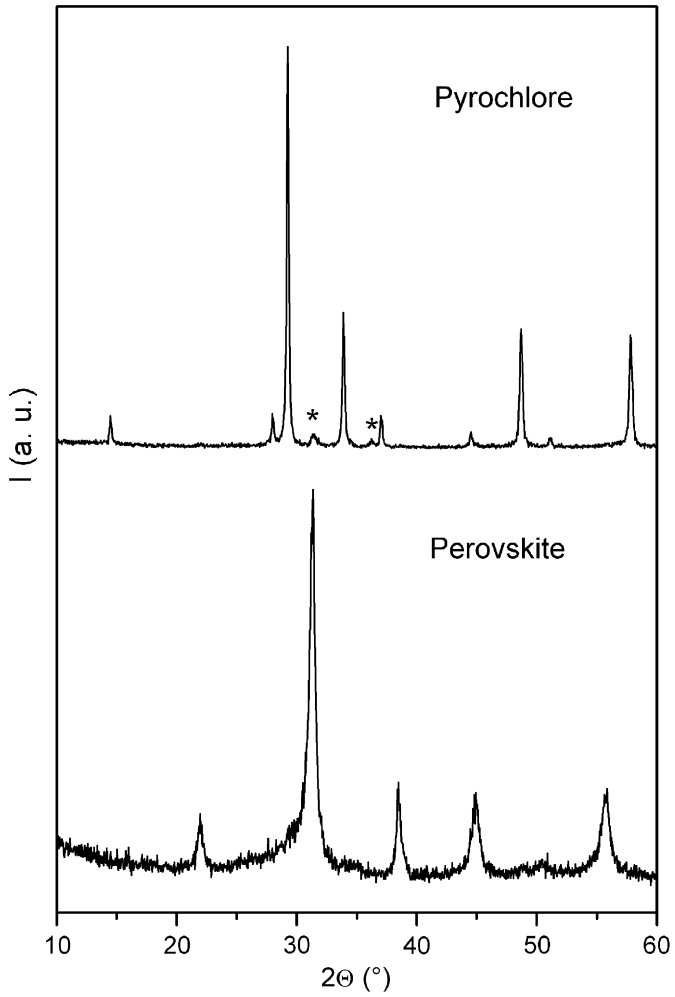

Fig. 4. XRD patterns of the 0.92PZN–0.08PT mechanosynthesized perovskite: (a) unannealed and (b) after thermal treatment at 700 °C (* = secondary phases: perovskite and ZnO).

Table 2
Unit-cell parameters of the different PZN–PT phases obtained by mechanosynthesis unannealed and after thermal treatment at 700 °C

Phase	Space group	a (Å)	V (Å^3)	V per ABO_3 formula (Å^3)
Perovskite	*Pm*3*m*	4.04(2)	66.0(4)	66.0(4)
Pyrochlore	*Fd*3*m*	10.578(5)	1183.7(5)	73.9(1)

The high instability of the PZN and PZN–PT perovskite and the decomposition in pyrochlore with temperature has been extensively described in the literature [10,18–20]. This behavior has been confirmed by the study of the variation of the free energy with temperature in the case of perovskite and pyrochlore phases of the PZN system. It can be observed that perovskite is only stable at room temperature and pyrochlore presents a lower free energy at a higher temperature [21]. So from a thermodynamical point of view, it is reasonable to assume that it is an easy transition.

Following the works of Andersson et al. [16] and Hyde and Andersson [22,23] various IPMS have turned out to be particularly useful for the description of many crystal structures and for perovskite and pyrochlore networks (*Pm*3*m* and *Fd*3*m* space groups, respectively). These structures can be described in terms of IPMS by the Schwarz P- and F-surface shown in Fig. 5a and c, respectively [24].

In the cubic (Pb*E*)MO_3, Pb*E* occupies a volume centred around the $\frac{111}{222}$ position in a simple MO_3 network (ReO_3 type) which is fitted to one side of the P-surface (Fig. 5a). The $[M_2O_6]$ network of the cubic $(PbE)_2M_2O_6$ pyrochlore is situated on one side of the F-minimal surface (Fig. 5c) Pb*E* fitting simply into the labyrinths defined by this surface. Note that in the mineral pyrochlre there is one fluorine (roughly the size of an oxygen) in the cavities centred on site 8*b* of the labyrinths, the Na and Ca lie in the sites 16*d*. In our case we have to locate at least two lone pairs in these cavities, Pb atoms being in 16*d*.

It is also worth pointing out that the cubic form of antimony oxide $Sb_2O_3E_2$ shows the same F-surface, its network resulting from a stacking of $Sb_4O_6E_4$ molecules (Fig. 6a) in which Sb atoms have the classical one-sided coordination scheme CN = 3+1, three oxygens and *E* making up a tetrahedron [25]. In this case the octahedra formed by the oxygens within the molecules are empty and create the same network as $[Nb_2O_6]$ in the mineral, Sb*E* pointing to the other side of the minimal surface, i.e. towards the labyrinths. In this space, four Sb*E* pertaining to four different $Sb_4O_6E_4$ molecules make a tetrahedron, the lone pairs pointing toward each other, (see Fig. 6b). Sb–Sb interatomic distances are 4.258 Å and according to previous studies on the localization of *E*, here Sb–*E* being at 1.06 Å, the distance E–E = 2.52 Å is in good agreement with their attributed size [15].

With respect to the position of Pb in site 16*d* of pyrochlore it should be pointed out that Pb is surrounded by six oxygens at Pb–O = 2.71 Å forming a very flat, distorted triangular antiprism (Fig. 7a). These PbO_6 polyhedra at the summits of the tetrahedron formed by Pb atoms define the large cavities centred on site 8*b*. Their large triangular bases, only 0.795 Å apart, separating the cavities exhibit major O–O distances around 4.643 Å, whereas the distance between the oxygens of the PbO_6 antiprism is equal to 2.796 Å. Another important distance is that between the gravity

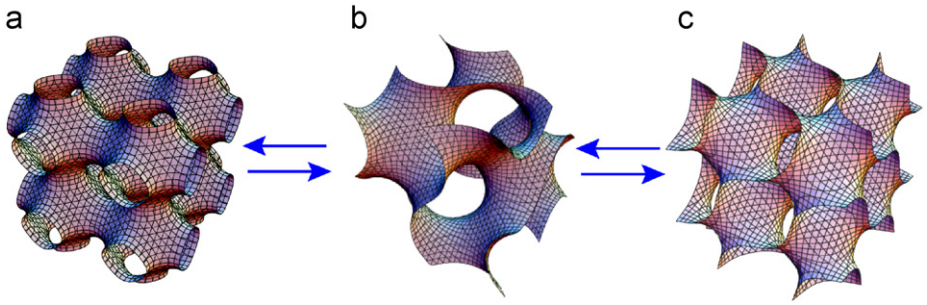

Fig. 5. Infinite periodic minimal surfaces: (a) for P-type perovskite structure, (b) for G-type gyroid, and (c) for F-type pyrochlore structure. Courtesy of Prof. S. Andersson (Sandvik Institute, Öland, Sweden).

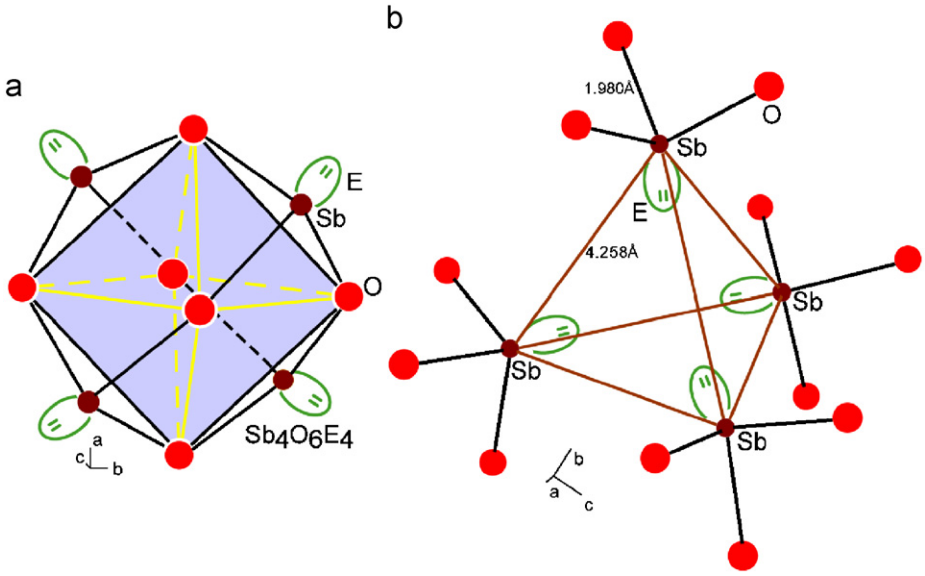

Fig. 6. (a) $Sb_4O_6E_4$ molecule and (b) tetrahedral space filled up by lone pairs into the labyrinths resulting from the stacking of four $Sb_4O_6E_4$ molecules.

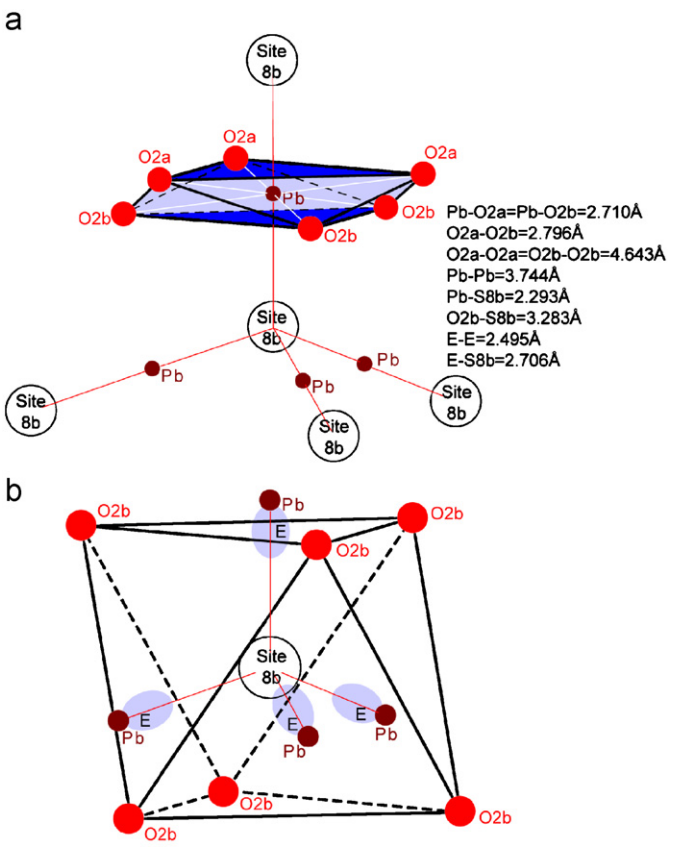

Fig. 7. (a) PbO_6 triangular antiprism: the two large triangular faces are dark blue. The Pb_4 tetrahedron is centred on the empty crystallographic site 8*b* and (b) the regular octahedron formed by the O2*b* oxygens encapsulating the four lone pair atoms of the Pb_4 tetrahedron. Blue form attached to Pb stands for lone pair *E*.

centre of the large triangles to oxygens O 2*a*, i.e. 2.681 Å; in other words, this large triangle could accommodate a sphere, the size of an oxygen or a lone pair, in its centre. Therefore it may be assumed that Pb*E* could easily flip and alternatively point its lone pair towards one cavity or to the adjacent one. The tetrahedron constituted by Pb atoms presents Pb–Pb distances of approx. 3.744 Å.

In this tetrahedron, at least two *E* must be located but it seems reasonable to propose as many as four *E* (Fig. 7b). If *E* is located ~0.8 Å from Pb in the direction of site 8*b*, the *E*–*E* distances remain reasonable E–$E = 2.5$ Å. This *E* packing is not uncommon in the case of Sb_2O_3 [25] but has also been found in As_2O_3, $TeCl_4$ [26], and $Sn_4O_2F_4$ [27]. Also, Pb can move slightly towards the centre of the large triangular base of its triangular antiprism and adopt a classical CN = 3+1 as *E* can come closer to the oxygen triangle. The change between the extremely dense packing in the case of the perovskite, with almost no space for the lone pairs, and the large cavities present in the case of the pyrochlore, allows us to understand the perovskite ⇒ pyrochlore phase transition and the explosion derived from it: the hypothesis is based on the important change in volume occurring over a very short period of time in a system under quite a high pressure, so the graphite die cannot resist the increase in pressure associated with this phenomenon, resulting in its blow-out.

Thus, as underlined above this transition is accompanied, by an extremely sudden expansion which leaves no time for the automatic pilot pressure system of the SPS machine to respond adequately. Then the graphite die containing the PZN–PT pellet explodes violently. This structural change requires, as usual, translation, rotation and reflection operations in conventional algebra but Hyde and Andersson have put forward a new concept based on differential geometry unifying the phenomenon into a single operation between two infinite periodic minimal surface. This concept was used to describe the martensitic transition austenite ⇒ metastable martensite, from an F-surface to the gyroid one (Fig. 5b) via the elliptic Bonnet transformation [23]. Bonnet transformation permits certain minimal surfaces to be transformed into others, with all intermediate surfaces being minimal surfaces. All intrinsic geometrical properties of the surfaces are preserved under the transformation. The transition from P-surface to F-surface can be obtained as in the case of the martensitic one via the Bonnet transformation. When the latter transformation occurs, it takes place almost instantaneously at various sites in the microcrystals, as in the case of the martensitic transformation. This mechanism is proposed in the reported experiment of PZN–PT sintering. Suddenly, all pellet crystallites change from perovskite to pyrochlore, with the corresponding

volume expansion, transforming the uniaxial pressure into a high isotropic pressure not supported by the die walls and leading to its explosion.

5. Conclusion

The "explosive" phenomenon during sintering of PZN–PT phase using SPS has highlighted the structural details directly linked to its perovskite ⇒ pyrochlore phase transition. Primarily emphasis has been placed on the importance of the lone pair volume in the expansion of the pyrochlore cell compared to the one of the perovskite, i.e. about 13%. Packing of the $[Sb_4O_6]$ molecules in the cubic senarmontite which shows the tetrahedral organization of the Sb^{3+} lone pairs *E* has been used as a model to propose a particular organization of Pb lone pairs in the large oxygenated cage of the pyrochlore structure centred on the empty site 8*b*. Inside this cage, the lone pairs *E* with their volume near oxygen are arranged in a tetrahedron and an increase of the volume per $PbMO_3$ unit is induced. Perovskite and pyrochlore structures can be described by the P-surface and the F-surface, respectively, and the transition between them can be explained by a single mathematical operation between these surfaces. The transformation between the two structures in the $PbZn_{1/3}Nb_{2/3}O_3$–$PbTiO_3$ system resembles an inverse martensitic transformation, as described by Hyde and Andersson through a Bonnet transformation from F-surface (fcc structure) to gyroid minimal surface (bcc packing of atoms), but in our case the sample has no time to adopt a stable structure described by a gyroid surface and moves directly from P- to F-IPMS.

Acknowledgments

The Centre National de la Recherche Scientifique (France) is gratefully acknowledged for its financial support. Dr. T. Hungría would also like to acknowledge the financial support of the Spanish MAE-AECI.

References

[1] S.E. Park, T.R. Shrout, Mater. Res. Innov. 1 (1997) 20–25.
[2] N. Setter (Ed.), EPFL, Lausanne, Switzerland, ISBN: 2-9700346-0-3, 2002.
[3] J. Kuwata, K. Uchino, S. Nomura, Ferroelectrics 37 (1981) 579–582.
[4] J.S. Forrester, E.H. Kisi, K.S. Knight, C.J. Howard, J. Phys.: Condens. Matter 18 (2006) L233–L240.
[5] B. Noheda, J. Gonzalo, L.E. Cross, R. Guo, S.E. Park, D.E. Cox, G. Shirane, Phys. Rev. B 61 (2000) 8687–8695.
[6] H.X. Fu, R.E. Cohen, Nature 403 (2000) 281–283.
[7] B. Noheda, D.E. Cox, G. Shirane, S.E. Park, L.E. Cross, Z. Zhong, Phys. Rev. Lett. 86 (2001) 3891–3894.
[8] N. Wakiya, N. Ishizawa, K. Shinozaki, N. Mizutani, Mater. Res. Bull. 30 (1995) 1121–1131.
[9] T. Fujiu, A. Tanaka, T. Takenaka, Jpn. J. Appl. Phys. 30 (1991) L298–L301.
[10] M. Algueró, J. Ricote, A. Castro, J. Am. Ceram. Soc. 87 (2004) 772–778.
[11] T. Hungría, M. Algueró, A.B. Hungría, A. Castro, Chem. Mater. 17 (2005) 6205–6212.
[12] T. Hungría, M. Algueró, A. Castro, J. Am. Ceram. Soc. 90 (2007) 2122–2127.
[13] M. Algueró, T. Hungria, H. Amorin, J. Ricote, J. Galy, A. Castro, Small 3 (2007) 1906–1911.
[14] S. Andersson, A. Aström, J. Galy, G. Meunier, J. Solid State Chem. 6 (1973) 187–190.
[15] J. Galy, G. Meunier, S. Andersson, A. Aström, J. Solid State Chem. 13 (1975) 142–159.
[16] S. Andersson, S.T. Hyde, H.G. von Schnering, Z. Kristallogr. 168 (1984) 1–17.
[17] Y. Kuroiwa, S. Aoyagi, A. Sawada, J. Harada, E. Nishibori, M. Takata, M. Sakata, Phys. Rev. Lett. 87 (2001) 217601.
[18] J.M. Hayes, T.R. Gururaja, G.L. Geoffroy, L.E. Cross, Mater. Lett. 5 (1987) 396–400.
[19] T.R. Gururaja, A. Safari, A. Halliyal, Am. Ceram. Soc. Bull. 65 (1986) 1601–1603.
[20] H.M. Jang, K.M. Lee, M.H. Lee, J. Mater. Res. 9 (1994) 2634–2644.
[21] N. Wakiya, N. Ishizawa, K. Shinomki, N. Mizutani, Mater. Res. Bull. 30 (9) (1995) 1121–1131.
[22] S.T. Hyde, S. Andersson, Z. Kristallogr. 168 (1984) 221–254.
[23] S.T. Hyde, S. Andersson, Z. Kristallogr. 174 (1986) 225–236.
[24] S. Andersson, K. Larsson, M. Larsson, M. Jacob, Biomathematics, Elsevier Sciences B.V., Amsterdam, 1999, p. 48.
[25] C. Svensson, Acta Crystallogr. B 30 (1974) 458–460.
[26] B. Bruss, B. Krebs, Inorg. Chem. 10 (1971) 2795–2800.
[27] B. Darriet, J. Galy, Acta Crystallogr. B 33 (1977) 1489–1492.